Plasma polarization spectroscopy of atomic and molecular emissions from magnetically confined plasmas

AUTHOR(S):

Shikama, T.; Fujii, K.; Kado, S.; Zushi, H.; Sakamoto, M.; Iwamae, A.; Goto, M.; Morita, S.; Hasuo, M.

CITATION:

Shikama, T. ...[et al]. Plasma polarization spectroscopy of atomic and molecular emissions from magnetically confined plasmas. Canadian Journal of Physics 2011, 89(5): 495-501

ISSUE DATE:

2011-05

URL:

http://hdl.handle.net/2433/152188

Plasma polarization spectroscopy of atomic and molecular emissions from magnetically confined plasmas

T. Shikama, K. Fujii, S. Kado, H. Zushi, M. Sakamoto, A. Iwamae, M. Goto, S. Morita, and M. Hasuo

Abstract: In spectroscopic measurements of magnetically confined torus plasmas, the line-integrated emission along a viewing chord is usually observed. However, by utilizing the dependence of the magnitude of the Zeeman splitting on the emission location, a few localized emissions existing along the viewing chord can be separated. Detailed analysis of the Zeeman split spectral line shapes then makes it possible to evaluate the local values of the magnetic field strength, population density, temperature, and flow velocity. We have introduced polarization spectroscopy to improve the accuracy in separating the overlapped spectra. The polarization resolved H_α, He I, and H_2 Fulcher-α band spectra are measured in TRIAM-1M tokamak, and atomic and molecular dynamics is investigated. Further progresses in the simultaneous measurements of the Balmer series and Fulcher-α band spectra in LHD and extension to the CH Gerö band spectra are briefly presented.

PACS Nos.: 52.25.Os, 52.25.Ya, 52.40.Hf, 52.55.Fa, and 52.55.Hc

Résumé: French version of abstract (supplied by CJP)

[Traduit par la rédaction]

1. Introduction

In magnetic fusion devices, the understanding of the neutral dynamics, namely, spatial distribution of the density, temperature, and flow velocity of atoms and molecules, is an important issue to achieve better core plasma confinement and steady state operation. The particle control including the helium ash pumping and wall recycling is a task to be investigated in ITER (*e.g.* [1]). Direct measurements of the atomic dynamics may enable us to quantitatively confirm the efficiencies of the helium pumping and hydrogen refueling. Meanwhile, it has been revealed that the recycling as well as the radiation safety is affected by the trapped hydrogen atoms and molecules in the carbon co-deposition layer. Formation and redeposition processes of hydrocarbon molecules in the vicinity of the carbon-fiber-composite as

Received . Accepted .

T. Shikama and K. Fujii. Graduate School of Engineering, Kyoto University, Kyoto 606-8501, Japan
S. Kado. School of Engineering, The University of Tokyo, Tokyo 113-8656, Japan
H. Zushi and M. Sakamoto. Research Institute for Applied Mechanics, Kyushu University, Kasuga, Fukuoka 816-8580, Japan. (M. Sakamoto's present affiliation is Plasma Research Center, University of Tsukuba, Tsukuba, Ibaraki 305-8577, Japan.)
A. Iwamae. Japan Atomic Energy Agency, Naka, Ibaraki 311-0193, Japan
M. Goto and S. Morita. National Institute for Fusion Science, Toki, Gifu 509-5292, Japan
M. Hasuo. Graduate School of Engineering, Kyoto University, Kyoto 606-8501, Japan

 DOI: 10.1139/Z*xx-xxx*

well as the absorption and desorption of hydrogen atoms and molecules in the co-deposition layer should be clarified.

The neutral behavior can be measured nearly only by spectroscopy which provides the line-integrated data along viewing chords. To perform the local measurements, the aid of other methods such as laser injection, local gas puffing, or adjustment of the viewing chords are usually required. As an alternative way of the local measurements, a technique based on high-resolution spectroscopy combined with analysis of the Zeeman patterns appearing in the emission line shapes has been developed. The Zeeman splitting of the spectra provides the information regarding the magnetic field strength at the brightest position. If the emission is localized, and the spatial distribution of the external magnetic field is present and known, one can deduce the emission position and the local values of the population density, temperature and flow velocity. This technique was applied to the H_α spectra [2] in a situation where one can assume one emission location along the viewing chord, and then extended to the D_α [3, 4] and He I $2^1\mathrm{P} - 3^1\mathrm{S}$ and $2^1\mathrm{P} - 3^1\mathrm{D}$ [5] spectra with two emission locations at the inboard and outboard sides of the torus. We have introduced polarization spectroscopy to further improve the accuracy in separation of the superposed spectra [6, 7]. In this paper, we review application results of the technique with the aid of polarization spectroscopy to atomic and molecular spectra in TRIAM-1M tokamak. We also briefly introduce recent results of the simultaneous observation of atomic and molecular spectra in LHD and extension to hydrocarbon molecular spectra.

2. Zeeman splitting of spectra

2.1. H_α and He I spectra

The Zeeman split atomic spectral line shapes are calculated based on quantum mechanical perturbation theory. Details of the calculation are described in elsewhere (*e.g.* [6, 8, 9]). The requirement to separate the superposed spectra which originate from the inboard and outboard sides can be approximately estimated from a relation

$$\Delta\lambda_{B(\mathrm{in})} - \Delta\lambda_{B(\mathrm{out})} > \Delta\lambda_0, \tag{1}$$

where $\Delta\lambda_{B(\mathrm{in})}$ and $\Delta\lambda_{B(\mathrm{out})}$ are the wavelength shifts by the Zeeman effect at the inboard and outboard emission positions, respectively, and $\Delta\lambda_0$ is the convoluted width of the Doppler broadening and instrumental function. In a high electron density regime, one may need to consider the Stark broadening, which is negligible in the present case. Under a magnetic field strength of larger than 1 T, hydrogen and helium spectra are in the Paschen-Back limit. The magnitude of the wavelength shift $\Delta\lambda_B$ for the σ transition can be approximated as $\Delta\lambda_B \simeq \mu_B|\boldsymbol{B}|\lambda_0^2/hc$, where μ_B is the Bohr magneton, $\boldsymbol{B}$ is the magnetic field, λ_0 is the vacuum wavelength of the emission, h is Planck's constant, and c is the velocity of light in vacuum. With sufficiently small instrumental function, the Doppler broadening becomes substantial. The above relation then leads to a requirement [6]

$$T < 3.67 \times 10^{11}(\lambda_0\Delta|\boldsymbol{B}|)^2 A, \tag{2}$$

where T is the temperature in eV, $\Delta|\boldsymbol{B}|$ is the difference of the magnetic field strength in Tesla, and A is the atomic mass number. For instance, when $\Delta|\boldsymbol{B}| = 0.5$-2 T, the estimated maximum temperature from eq. (2) is 0.04-0.6 eV for the H_α emission (656 nm) and 0.1-2 eV for the He I $2^3\mathrm{P} - 3^3\mathrm{D}$ emission (588 nm). Separate observation of only the σ spectra approximately doubles the quantity $\Delta\lambda_B$ and increases the tolerable maximum temperature four times. Polarization spectroscopy thus enables the separation of the spectra in wider experimental conditions.

2.2. H_2 Fulcher-α band spectra

For the calculation of the Zeeman effect on the H_2 Fulcher-α ($d^3\Pi_u - a^3\Sigma_g^+$) band spectra, the effective Hamiltonian including the energies of the centrifugal distortion, spin-orbit interaction, and

Zeeman effect besides the ro-vibronic energy is adopted. Inclusion of these terms gives sufficient accuracy compared to typical experimental resolution of visible emission spectroscopy. The ro-vibronic emission intensity is evaluated under the Born-Oppenheimer approximation. Detailed formulation and generalization to other diatomic molecules are summarized in [10,11]. The Zeeman split in the Fulcher-α band spectra is in the Paschen-Back limit. The magnitude of the wavelength shift $\Delta\lambda_B$ for the π transition in the rotational bandhead can be approximated as $\Delta\lambda_B \simeq \mu_B|\boldsymbol{B}|\lambda_0^2/2hc$. The Doppler broadening of molecules is usually negligible, and the requirement for the separation of the spectra can be estimated in terms of $\Delta|\boldsymbol{B}|$ and instrumental function in eq. (1). For instance, $\Delta|\boldsymbol{B}| =$ 1-2 T requires an instrumental width of 0.008-0.017 nm. Observation of only the π spectra makes the tolerable instrumental width twice.

3. Experiments

TRIAM-1M tokamak [15] has a major radius of 0.84 m and minor radius of about 0.12 m. The magnetic field strength of about 6.7 T at the plasma center is generated using sixteen toroidal field coils. The plasma boundary shape is restricted by three D-shaped poloidal limiters and one vertically movable limiter installed in the upper port of the vacuum vessel. For experiments with a single-null magnetic field configuration, toroidal divertor plates are installed at the bottom of the vessel in such a way that the surface of the divertor plate is aligned with that of the D-shaped limiters. All the plasma-facing components are made of molybdenum. Discharges discussed in this paper were conducted in limiter configurations. The last closed flux surface (LCFS) was determined by the D-shaped limiter in the case of atomic emission measurements, while that was determined by the movable limiter inserted to about $y = 100$ mm (Fig. 1) in the case of molecular emission measurements. The plasma was initiated by ohmic and then sustained by 8.2 GHz lower hybrid current drive (LHCD). During the LHCD phase, the plasma current was 40 kA, electron temperature at the plasma center was about 1 keV, line averaged electron density was 1×10^{19} m^{-3}, and neutral pressure at the bottom of the vessel was about 10 mPa.

Atomic emissions generated around the LCFS were observed using fan-shaped 25 radial viewing chords with a spot diameter of about 5 mm as shown in Fig. 1. A linear polarizer (OFR PUM-15) was attached in front of the objective lenses with the polarization axis perpendicular to the toroidal field direction. Due to the weak poloidal field, the magnetic field pitch angle at the LCFS was smaller than 1 degree, so that only the σ polarization components can be resolved with sufficient extinction ratio. The viewing chords are numbered one to twenty-five from the top to bottom. The H_2 molecular emission generated in the vicinity of the movable limiter surface was observed from the bottom of the chamber through the plasma using a radial viewing chord with a spot size of about 35 mm on the limiter surface. In front of the objective lens, a UV sharp-cut filter (Sigma Koki SCF-42L) and a linear polarizer (Sigma Koki NSPFU-30C) were installed. The collected emission was dispersed using a Czerny-Turner mounted spectrometer (Acton Research AM-510) which has a focal length of 1 m and 1800 grooves/mm ruled grating. Astigmatism compensation optics consisting of two concave mirrors was installed at the entrance of the spectrometer. The dispersed spectrum was detected using a back-illuminated CCD (Andor DU440-BU2) which has a dynamic range of 16 bits and 2048 $\times$ 512 pixels with a size of 13.5 $\times$ 13.5 μm^2. For atomic spectra, the slit width was set to 15 μm. The reciprocal linear dispersion was 0.404 nm/mm at 656 nm, and wavelength resolution was 0.015 nm at the FWHM. On the other hand, for molecular spectra, the slit width was set to 80 μm having given a reciprocal linear dispersion of 0.426 nm/mm at 602 nm and wavelength resolution of 0.035 nm.

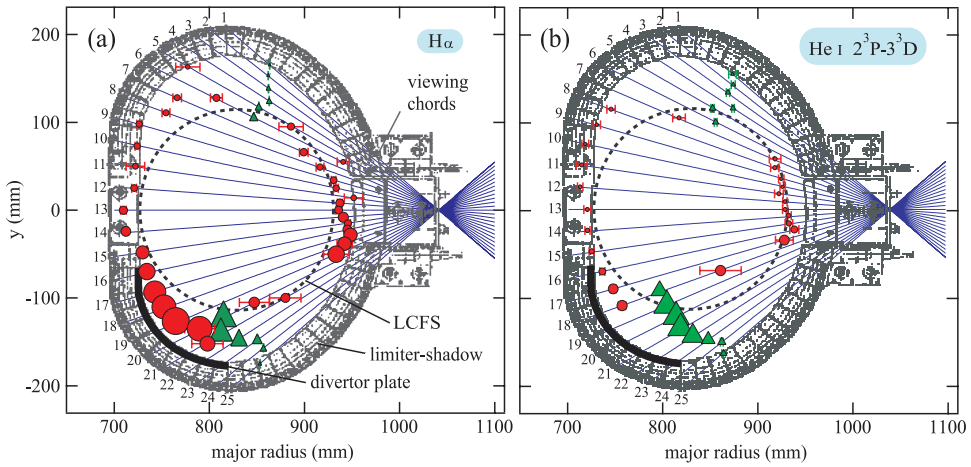

Fig. 1. Emission intensity distributions of (a) H_α and (b) He I cold temperature components. The filled circles denote the positions obtained with assuming two emission positions, and the filled triangles denote those obtained with assuming one emission position. The diameter of the marker indicates the relative emission intensity, and the horizontal bar shown with the marker is the standard deviation of the emission position.

4. Application to H_α and He I spectra

4.1. Emission intensity distribution

Fig. 2(a) shows the observed σ spectrum of the H_α emission on the midplane viewing chord (ch 13 in Fig. 1) [9]. One can see asymmetry in the spectrum which is caused by the overlapping of the Doppler shifted spectra originating from the inboard and outboard sides. To carry out the fitting to the experimental data, we approximately classified the temperature of hydrogen atoms into three categories: cold (< 1 eV), warm (1-10 eV), and hot (> 10 eV). These components may be attributable to atoms produced by different processes like recombinations, dissociations [16], charge-exchanges [17], and surface reflections [18]; however, validity of this simplification should be elaborated in the future. In the fitting procedure, two cold and two warm components, and one hot component were assumed. We assumed the same emission position of the inboard or outboard side for the cold and warm components for simplicity. For the hot component, separation between the inboard and outboard sides is difficult because of the larger Doppler broadening than the Zeeman splitting. Each temperature component consists of thirty Zeeman split fine structure transitions. Consequently, the number of fitting parameters are eighteen, *i.e.* two magnetic field strengths, five peak intensities, five Doppler widths, five Doppler shifts, and one background level. The fitting results are indicated by lines in the figure. On the peripheral viewing chords, symmetric σ spectra were observed as shown in Fig. 2(b). We can assume one emission location on these chords. The number of fitting parameters are then eleven, *i.e.* one magnetic field strength, three peak intensities, three Doppler widths, three Doppler shifts, and one background level.

The fitting for the warm and hot components is mainly determined from the shoulder and pedestal of the spectrum, and the evaluated parameters have relatively large uncertainties. Meanwhile, that for the cold components is determined from the peak shape, and in particular the Zeeman splitting and Doppler shift have small uncertainties. We therefore discuss the cold temperature components hereafter. The determined emission positions of the cold components are shown in Fig. 1 (a). The markers indicate the emission positions, and the diameter of the marker represents the relative emission intensity. The horizontal bar shown with the marker is the standard deviation of the determined emission po-

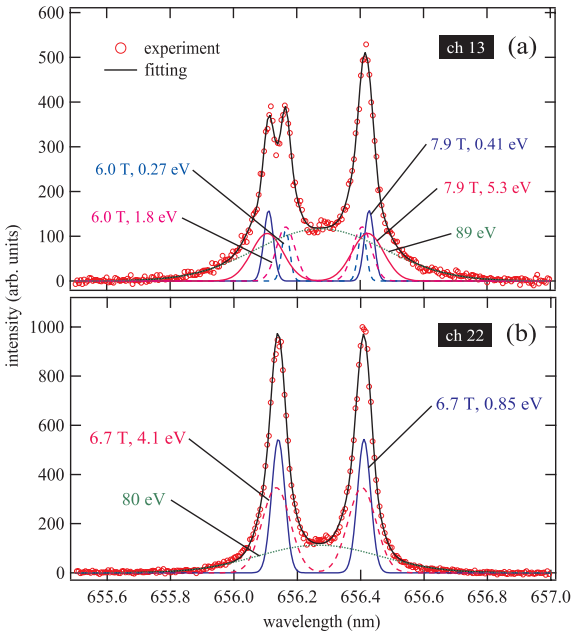

Fig. 2. H_α σ spectra measured on the (a) midplane (ch 13) and (b) peripheral (ch 22) viewing chords. The open circles denote the observed spectra, and the lines denote the fitting results assuming three temperature components.

sition. The circles denote the positions obtained with assuming two emission positions, while triangles denote those obtained with assuming one emission position. One can see that the emission positions are around the LCFS. At the inboard side, the emissions originate from the region between the vacuum vessel and the poloidal limiter surface, the so-called limiter-shadow. The larger emission intensities at the bottom of the vessel are due to the recycling flux from the divertor plate. Though the present experiments were carried out in limiter configurations, the plasma influx to the divertor plate was confirmed from the molybdenum atomic emission along the divertor plate [9]. The emission positions inside the LCFS were determined on viewing chords ch 6, 7, 8, and 20. These are probably misfitting because of the elongation of the emission region along the viewing chord which will be mentioned below. We have conducted similar measurements for the He I $2^3P - 3^3D$ transition by puffing helium gas into the hydrogen discharge. The evaluated emission positions are similar to those of the H_α as shown in Fig.1 (b). Spatial asymmetry of the intensity distribution is larger in the case of helium. The emission distributions of the H_α and He I spectra around the LCFS were also obtained in LHD [5, 12–14].

The spatial resolution of the measurements is specified by the spot size of the viewing chord, fitting error, and broadening of the emission region. In the present measurements, the size of the viewing spot is about 5 mm, and the fitting error is less than 10 mm around the midplane. The broadening of the emission region can be deduced from the difference of the spectral widths between the π and σ components because the latter can be broadened by the integration of the Zeeman shift over the emission region. In our experiments, however, the estimation has difficulty because of the overlapping of the Doppler shifted spectra and existence of the multiple temperature components. In LHD, the broadening was evaluated to be about 50 mm (minor radius is 0.54-0.64 m) for the polarization un-resolved He I $2^1P - 3^1S$ spectra because the spectra can be fitted only by the cold temperature components [5]. The broadening of the emission region may become smaller in the devices which have steeper electron temperature and density gradients like ITER.

4.2. Flow velocity

The flow velocities of the cold temperature components were measured from the Doppler shifts of the separated spectra [9]. Fig. 3 shows the spatial profile of the measured flow velocities of hydrogen atom cold temperature components as projections on the viewing chords. We take the sign of the velocity such that a positive value denotes the red-shift of the spectrum directing toward the inboard side (away from the observer), while a negative value denotes the opposite. The flow profile indicates a radial inward flow, which can be explained by the initial velocity and momentum balance. Here one should bear in mind that the initial velocity when the atoms are released from the wall directs inward. The toroidal and poloidal flows are driven by the ion-atom friction force along the magnetic field and in the direction of the cross-field ion drifts, respectively, in which the momentum is transferred by the charge-exchange and elastic collisions. The radial flow is driven by the inward radial atomic pressure gradient and outward friction force due to the diffusion of ions. In TRIAM-1M, electron density in the SOL is lower than 10^{18} m^{-3}, so that ion-atom friction force is small [9]. In fact, the observed velocity profile cannot be explained by the toroidal or poloidal flow which should become zero on the midplane viewing chord (ch 13). We, therefore, conclude that the flow is generated by the radial atomic pressure gradient. At the bottom of the chamber, the flow velocity is significantly affected by the radial position of the magnetic axis. The inward shift of the axis gives the larger plasma influx toward the divertor plate which results in the larger recycling flux and larger flow velocity, while the outward shift gives the opposite. Note that in the case of the helium emission, smaller velocity was observed [9]. Provided that the pressure profile was not largely varied by the gas injection, this is consistent with a fact that the pressure gradient force is inversely proportional to the mass. Similar flow profile was observed in LHD under similar electron density in the emission region [13]. In contrast, in Alcator C-Mod tokamak, the toroidal flow was dominated because of the larger electron density up to 10^{20} m^{-3} [4].

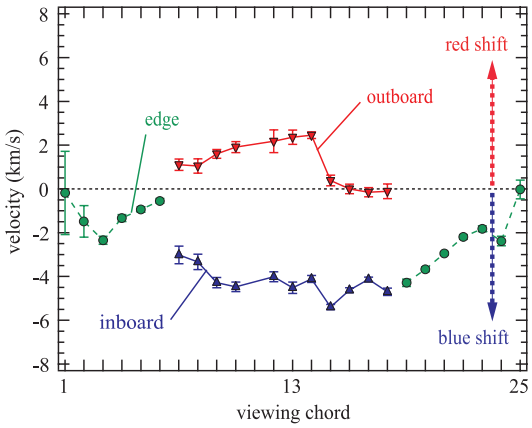

Fig. 3. Flow velocity profile of the hydrogen atom cold temperature components. The filled triangles are evaluated from the fitting results with assuming two emission locations, while the filled circles are evaluated from those assuming one emission location. The positive velocity indicates the direction toward the inboard side, and the negative velocity indicates the opposite.

5. Application to H_2 Fulcher-α band spectra

The H_2 Fulcher-α band spectra generated in the vicinity of the movable limiter surface were measured [10]. We adopted a simple viewing geometry with one emission position along the viewing chord. The Q-branch rotational transitions up to $N = 5$ in vibrational diagonal transitions up to $v = 2$ were observed using three identical discharges because of the limitation of the measurable wavelength range

(about 12 nm per CCD frame), where v and N are the vibrational and rotational quantum numbers, respectively. In Fig. 4, the π and σ spectra of the $v' = v'' = 0$ transition are shown, where prime and double prime denote the upper and lower states, respectively. The magnetic field strength of 6.7 T was deduced from the Zeeman splitting of the $Q1$ spectrum π component. The broadening of the emission region can be deduced from the widths of the π and central components of the σ spectra. However, because of the low S/N ratio of the spectra, the evaluation is difficult. We simply assume that the evaluated emission position reflects the peak position of the emission within the viewing spot. The evaluated magnetic field strength corresponds to a major radius of 838 mm, and the position coincides with that of the magnetic axis. This means that the emission originates from the point where plasma contacts with the limiter surface. The ro-vibrational temperatures in the $X^1\Sigma_g^+$ state were estimated based on the measured population distribution in the d-state and coronal model analysis [10]. The evaluated vibrational temperature was around 3300 K and almost constant during the discharge. On the other hand, an increase in the rotational temperature from 700 to 900 K accompanying the discharge duration was observed. The increase is explained by the rise in the surface temperature [20].

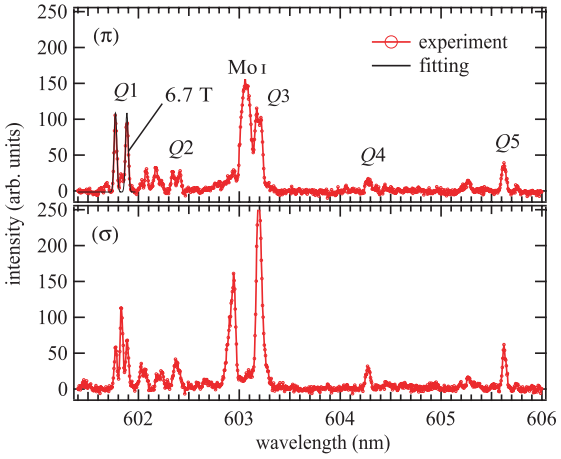

Fig. 4. π and σ polarization components of the Fulcher-α band spectra ($v' = v'' = 0$). The open circles denote the experimental data, and the line at the $Q1$ spectrum π-component denotes the fitting result.

6. Recent progresses

6.1. Simultaneous measurements of Balmer series and Fulcher-α band spectra in LHD

For the simultaneous observation of the Balmer series and Fulcher-α band spectra, we have developed a multiwavelength-range fine-resolution spectrometer [12, 19]. The spectrometer has the Czerny-Turner configuration with a focal length of 1.14 m equipped with a 2400 grooves/mm holographic grating. Five focusing mirrors are installed at the locations which correspond to the wavelengths of the H_α, H_β, and H_γ spectra, and Fulcher-α band Q-branch spectra with $v' = v'' = 0$ and $v' = v'' = 2$ transitions. The dispersed emission was detected by a CCD (Andor DV435-BV) which has a dynamic range of 16 bits and 1048 $\times$ 1048 pixels with a pixel size of 13 $\times$ 13 μm^2. The wavelength resolution was 0.007 nm at the wavelength of the H_α and 0.01 nm at the wavelength of the H_γ when we adopted a slit width of 30 μm.

A viewing chord was placed slightly above the midplane of LHD [21] passing through the regions close to two null-points. For the separation of the polarization components, we used polarization separation optics (PSO) [7] which consists of a Glan-Thompson prism and objective lenses. The sep-

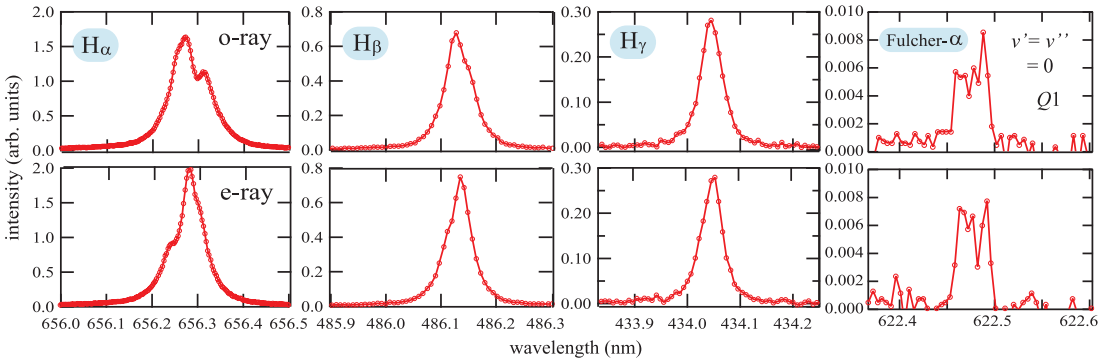

Fig. 5. Simultaneously observed H_α, H_β, H_γ, and Fulcher-α band $Q1$ ($v' = v'' = 0$) spectra. The upper and lower figures show the spectra of the o-ray and e-ray, respectively.

arated ordinary ray (o-ray) and extraordinary ray (e-ray) were transferred by different optical fibers. The difference of the magnetic field pitch angle between the inboard and outboard LCFS is close to 90 degree [7], so that we adjusted the axis of PSO such that the π and σ spectra from the inboard LCFS are detected as o-ray and e-ray, respectively. As a result, the o-ray mainly consists of the π spectrum from the inboard side and σ spectrum from the outboard side, while the π and σ spectra become vice versa for the e-ray. The measured H_α, H_β, H_γ, and Fulcher-α band ($v' = v'' = 0$) spectra are shown in Fig. 5. For the H_α spectra, the inboard and outboard emission locations consistent with the former results were evaluated [12].

6.2. Extension to CH Gerö band spectra

The technique is now under extension to the CH Gerö band ($A^2\Delta - X^2\Pi$) spectra [11, 22]. We constructed a calculation code which can calculate the Zeeman split spectral line shapes of diatomic molecules. The calculated CH spectra were verified by experiments using a pure methane glow discharge plasma installed in a superconducting magnet. The polarization resolved spectra were measured using a PSO from the direction perpendicular to the magnetic field direction. Fig. 6 shows the measured spectra under 0.0 and 1.5 T, and calculation results assuming a A-state vibrational temperature of 2600 K and rotational temperature of 730 K. One can see that both the results are in good agreement. A slight disagreement of the intensity blow 430.9 nm may originate from the deviation from the Boltzmann rotational population distribution. The calculation results predict the continuous change in the shape of the spectra by the Zeeman splitting up to larger N, so that the present technique is basically applicable. Verification in actual magnetic confinement devices is underway.

7. Conclusion

A spectroscopic technique for the local measurements of atomic and molecular emissions under strong magnetic field has been developed. By observing the polarization resolved spectra, the accuracy in detecting the magnitude of the Zeeman splitting and separating the superposed spectra was improved. The H_α and He I emissions around the LCFS were observed in TRIAM-1M tokamak, and the spatial asymmetry of the intensity was attributed to the recycling from the divertor plate. The radial inward atomic flows were detected from the Doppler shifts of the separated spectra, and we concluded that the flows are generated by the atomic pressure gradient. We also applied the technique to the H_2 Fulcher-α band spectra, and the emission position and local ro-vibrational temperatures in the vicinity

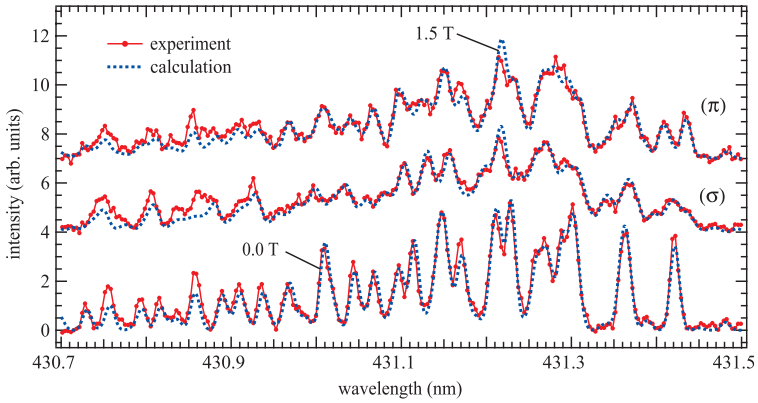

Fig. 6. Measured (open circles) and calculated (dashed lines) CH Gerö band Q-branch spectra under 0.0 and 1.5 T. In the calculation, a A-state vibrational temperature of 2600 K and rotational temperature of 730 K are assumed.

of the plasma facing components were evaluated. The technique was further extended to the simultaneous observation of the Balmer series and Fulcher-α band spectra in LHD, and applicability to the CH Gerö band spectra was confirmed in a basic experiment.

Acknowledgement

This work was supported by NIFS collaborative research program under Grant No.NIFS04KUTR001 and NIFS08KOAP020, collaboration program of Research Institute for Applied Mechanics in Kyushu University, and Grant-in-Aid for Scientific Research (B) under Grant No.21340170 and Grant-in-Aid for Young Scientists (B) under Grant No.22740362 from JSPS.

References

1. A. Loarte, B. Lipschultz, A. S. Kukushkin, *et al.*, *Nucl. Fusion* **47**, S203 (2007).
2. P. G. Carolan, M. J. Forrest, N. J. Peacock, and D. L. Trotman, *Plasma Phys. Control. Fusion* **27**, 1101 (1985).
3. J. L. Weaver, B. L. Welch, H. R. Griem, J. Terry, B. Lipschultz, C. S. Pitcher, S. Wolfe, D. A. Pappas, and C. Boswell, *Rev. Sci. Instrum.* **71**, 1664 (2000).
4. B. L. Welch, J. L. Weaver, H. R. Griem, W. A. Noonan, J. Terry, B. Lipschultz, and C. S. Pitcher, *Phys. Plasmas* **8**, 1253 (2001).
5. M. Goto and S. Morita, *Phys. Rev. E* **65**, 026401 (2002).
6. T. Shikama, S. Kado, H. Zushi, A. Iwamae, and S. Tanaka, *Phys. Plasmas* **11**, 4701 (2004).
7. A. Iwamae, M. Hayakawa, M. Atake, and T. Fujimoto, *Phys. Plasmas* **12**, 042501 (2005).
8. M. Goto, "Zeeman and Stark Effects" in "Plasma Polarization Spectroscopy" ed. by T. Fujimoto and A. Iwamae, *Springer* (2008) pp.13-28.
9. T. Shikama, S. Kado, H. Zushi, M. Sakamoto, A. Iwamae, and S. Tanaka, *Plasma Phys. Control. Fusion* **48**, 1125 (2006).
10. T. Shikama, S. Kado, H. Zushi, S. Tanaka, *Phys. Plasmas* **14**, 072509 (2007).
11. T. Shikama, K. Fujii, K. Mizushiri, M. Hasuo, S. Kado, and H. Zushi, *Plasma Phys. Control. Fusion* **51**, 122001 (2009).
12. K. Fujii, K. Mizushiri, T. Nishioka, T. Shikama, A. Iwamae, M. Goto, S. Morita, S. Kado, K. Sawada, and M. Hasuo, *Rev. Sci. Instrum.* **81**, 0331106 (2010).
13. A. Iwamae, A. Sakaue, N. Neshi, J. Yanagibayashi, M. Hasuo, M. Goto, and S. Morita, *J. Phys. B: At Mol. Opt. Phys.* **43**, 144019 (2010).

14. K. Mizushiri, K. Fujii, T. Shikama, A. Iwamae, M. Goto, S. Morita, and M. Hasuo, *Plasma Phys. Control. Fusion* **53**, 105012 (2011).
15. H. Zushi, K. Nakamura, K. Hanada, *et al.*, *Nucl. Fusion* **45**, S142 (2005).
16. H. Kubo, H. Takenaga, T. Sugie, S. Higashijima, S. Suzuki, A. Sakasai, and N. Hosogane, *Plasma Phys. Control. Fusion* **40**, 1115 (1998).
17. B. Wan, J. Li, J. Luo, J. Xie, Z. Wu, and X. Zhang, *Nucl. Fusion* **39**, 1865 (1999).
18. R. Aratari and W. Eckstein, *Nucl. Instrum. Methods Phys Res. B* **42**, 11 (1989).
19. K. Fujii, T. Shikama, A. Iwamae, M. Goto, S. Morita, and M. Hasuo, *Plasma Fusion Res.* **5**, S2079 (2010).
20. T. Shikama, S. Kado, K. Kurihara, and Y. Kuwahara, *Phys. Plasmas* **16**, 033504 (2009) *and references therein*.
21. Special issue on large helical device (LHD), *Fusion Sci. Tech.* **58** (2010).
22. T. Shikama and M. Hasuo, *J. Nucl. Mater.* **415**, S1159 (2011).